Pure & Appl. Chem., Vol. 69, No. 11, pp. 2321–2328, 1997.
Printed in Great Britain.

Dynamic heat capacity and enthalpy relaxation of a supercooled liquid $[Ca(NO_3)_2]_{0.4}$ $[KNO_3]_{0.6}$

Il-Kwon Moon and Yoon-Hee Jeong

Department of Physics, Pohang University of Science and Technology
Pohang, Kyungbuk, 790-784, S. Korea

Abstract: The linear and nonlinear enthalpy relaxation of a supercooled liquid $[Ca(NO_3)_2]_{0.4}[KNO_3]_{0.6}$ in the glass transition region was investigated using the calorimetric methods such as modulation, scanning, and adiabatic ones. It is demonstrated that the nonlinear enthalpy relaxation of $[Ca(NO_3)_2]_{0.4}[KNO_3]_{0.6}$ in the glass transition region is fully accountable in terms of the equilibrium response function if the latter is properly extended.

INTRODUCTION

When a liquid is cooled below the freezing temperature, it usually undergoes a first-order phase transition into a crystal. However, there are many materials which can be easily supercooled mainly due to the fact that they have a large viscosity at the freezing temperature.(ref. 1) Although liquids under equilibrium conditions are considered as disordered arrangements, lacking a long-range order, of molecules, they still possess structures in the short range. However, these orders are not of static nature and consequently they appear as structural fluctuations. When the temperature of a liquid, for example, is changed, the structure of a liquid changes accordingly to the new equilibrium condition. While this *structural relaxation* occurs on a microscopic time scale in ordinary situations, slow relaxation manifests itself when a liquid is sufficiently cooled below the freezing temperature. Then the glass transition, the process of a sufficiently supercooled liquid becoming an amorphous solid, may simply be considered as a phenomenon of the relaxation time becoming longer, as the temperature is lowered at a certain rate, than the experimental time scale set by the cooling rate. One of the outstanding fundamental problems related to the glass transition, however, is whether this slowing down is of purely kinetic origin or due to an underlying thermodynamic transition.(ref. 2,3) Despite intensive research of many decades, it remains controversial.

In this paper, we report our investigation on various aspects (linear and nonlinear, and equilibrium and nonequilibrium) of relaxation phenomenon associated with the glass transition. It is our view that one would get better understanding of the fundamental nature of the glass transition by thoroughly studying kinetic relaxation processes in supercooled liquids. There are many ways to probe slow dynamics associated with the glass transition. One of more frequently used methods is the measurements of enthalpy relaxation. The standard method for the measurements of enthalpy relaxation has been rate-scanning experiments using a Differential Scanning Calorimeter (DSC). In these measurements, one measures the heat capacity of a system as a function of temperature under such a condition that the temperature of the system changes continuously at a constant rate (heating or cooling). Here the cooling (or heating) rate sets the experimental time scale, and the system falls from (or recovers) thermal (quasi-)equilibrium. In addition to the scanning measurements, one can also utilize modulation calorimetric techniques where one probes the linear response of the system to a very small ac heat variation. In these measurements, one measures dynamic heat capacity, which represents the dynamics of the system in equilibrium, as a function of frequency and temperature.

It is generally recognized that nonlinear relaxation is involved in the situation associated with the

rate scanning experiment. (See the next section.) On the other hand, the dynamic heat capacity measurements are done in the linear response regime. Thus, despite the fact that the two methods are probing the same enthalpy relaxation of a system, it is not obvious if these two methods yield the same information on the system. We shall show how the two methods are described in terms of the thermal response function of the system. Furthermore, we have explored in detail the nonlinearity of enthalpy relaxation by observing the temperature evolution in a sample, as a function of time, under adiabatic condition. All the measurements described in this paper were done with a canonical glass former $[Ca(NO_3)_2]_{0.4}[KNO_3]_{0.6}$ (CKN). CKN is a binary mixture which becomes an ionic liquid when melted. Since cations have spherical charge distributions and nitrate ions are of trigon shape, CKN represents one of simple systems which can stay undercooled for days without crystallization. This good glass-forming ability was essential for time-consuming measurements.

THERMAL RESPONSE FUNCTION

Heat capacity is given thermodynamically by $C_p = d\tilde{H}/dT$ where T and $\tilde{H}$ are the temperature and the enthalpy of a given system respectively. Now we wish to extend this definition to the dynamic regime. To do this, we resort to the general response equation:(ref. 4) The response $\epsilon(t)$ of a system to an external perturbation $\sigma(t)$ can be written as

$$\epsilon(t) = \int_{-\infty}^{t} K_1(t,t')\sigma(t')dt' + \int_{-\infty}^{t}\int_{-\infty}^{t} K_2(t,t',t'')\sigma(t')\sigma(t'')dt'dt'' + \cdots . \tag{1}$$

Here ϵ is any strain quantity, σ is an externally applied stress quantity, and K_1 and K_2 represent the response functions. Eq. (1) was derived under only two assumptions, *causality and analyticity*, and therefore is applicable to a variety of linear and nonlinear situations. From the statistical mechanical point of view, all the equilibrium or near-equilibrium properties of a system with a fixed volume are described as a function of $\mathcal{H}_0/k_BT$, where $\mathcal{H}_0$ is the Hamiltonian of the system and k_B is the Boltzmann constant. For a small temperature variation δT, the perturbing term in the Hamiltonian can be obtained from

$$\frac{\mathcal{H}_0}{k_B(T+\delta T)} \approx \frac{\mathcal{H}_0(1-\delta T/T)}{k_BT}. \tag{2}$$

Thus, the external perturbing field σ in our case is represented by $\delta T/T$ which couples to the Hamiltonian of the system in the fixed volume case. For an isobaric situation which is more common with condensed matter, $\delta T/T$ couples to enthalpy $H = \mathcal{H}_0 + PV$ where P and V denote pressure and volume respectively. Except for phenomena occurring at low temperatures $\delta T/T$ is usually small and we shall assume that only the first term in Eq. (1) is necessary. This is the assumption usually made in the literature, but the nonlinear effects in enthalpy relaxation due to the higher order terms may be possible. One of the purposes of the present investigation is to critically test this assumption.

For the isobaric thermal responses ϵ is taken to be the enthalpy change from the equilibrium value, $\delta < H >$, per unit mass and Eq. (1) becomes

$$\frac{\delta < H(t) >}{\rho V} = \int_{-\infty}^{t} K_H(t,t')\delta T(t')dt' + C_p^{\infty}\delta T(t) \tag{3}$$

where ρ is the density. Here we use enthalpy per unit mass and take δT as the perturbation instead of $\delta T/T$ following the usual definition of the specific heat capacity (= heat capacity per gram). C_p^{∞} represents the contribution from the fast degrees of freedom such as phonons and K_H is the response function due to the slow relaxation of the system. One also defines the relaxation function

$$R(t,t') = \int_{-\infty}^{t'} K_H(t,t'')dt'' \tag{4}$$

which represents the response of the system to a step-like stimulus. For the system in equilibrium the relaxation function has the property of being stationary, i.e., $R(t,t') = R(t-t')$. It should be noted here that the usual nonlinearity in enthalpy relaxation is caused by the lack of stationariness in most, perhaps all, cases and can be dealt with in terms of Eq. (3). This *nonstationary* relaxation is different from the higher order effects mentioned above. For equilibrium situations, it can be shown that

$$R(t) = \frac{< \delta H_R(t)\delta H_R(0) >}{k_BT^2\rho V} \tag{5}$$

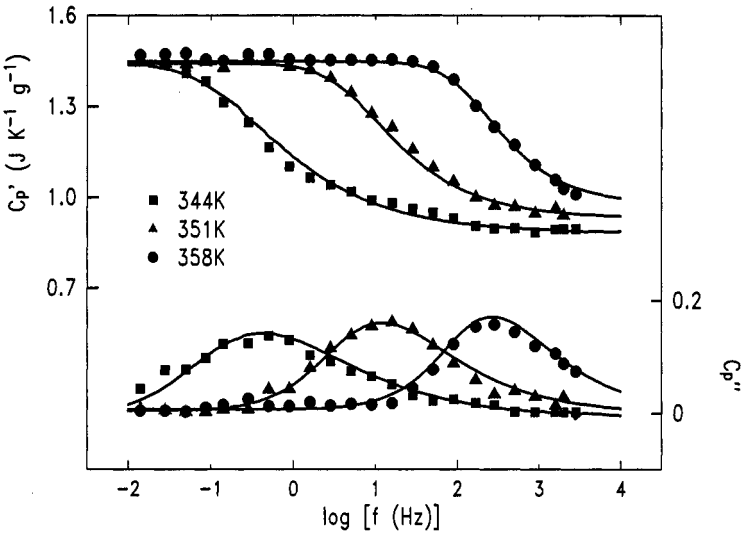

Fig. 1 The real and imaginary parts of specific heat capacity $C_p(\omega)$ of CKN as a function of frequency. The solid lines are fits to the data with a Kaulrausch-Williams-Watts function, $\exp[-(t/\tau)^{\beta}]$, with $\beta = 0.53$ (344 K), 0.57 (351 K), and 0.62 (358 K).

where δH_R represents the enthalpy fluctuation associated with the slow relaxation.(ref. 5)

In the frequency domain, that is, with the oscillating perturbation $\delta T \sim \exp(i\omega t)$, the dynamic heat capacity with real and imaginary parts, $C_p(\omega) = C_p'(\omega) - iC_p''(\omega)$, may be expressed in terms of the one-sided Fourier transform of either the response function $K_H(t)$ or the time derivative of the relaxation function $R(t)$ from Eq.(3):

$$C_p(\omega) = \int_0^{\infty} K_H(t)\, e^{-i\omega t}\, dt + C_p^{\infty} = \int_0^{\infty} [-dR(t)/dt]\, e^{-i\omega t}\, dt + C_p^{\infty}. \tag{6}$$

Since $R(t)$ is given by the enthalpy-enthalpy correlation function, $C_p(\omega)$ can be written as

$$C_p(\omega) = C_p^0 - \frac{i\omega}{k_B T^2 \rho V} \int_0^{\infty} dt\, e^{-i\omega t} < \delta H_R(0) \delta H_R(t) > \tag{7}$$

$C_p^0 = C_p^{\infty} + R(0) = C_p^{\infty} + < \delta H_R^2 > / k_B T^2 \rho V$. Thus, the slow relaxation of enthalpy governed by the system dynamics is the origin of the frequency-dependent heat capacity and therefore one can probe the slow dynamics of the system by measuring the dynamic heat capacity.

DYNAMIC HEAT CAPACITY OF CKN

For the measurements of the isobaric dynamic specific heat capacity, $C_p(\omega)$, of CKN we used the fully automated dynamic calorimeter developed in this laboratory.(ref. 6) Due to the space limit, we refer the reader to ref. 6 for details. Briefly, the calorimeter adopts the 3ω modulation technique,(ref. 7) which is an ac-method that uses a heater, which is in contact with a liquid sample, as a sensor simultaneously. By measuring the temperature oscillation of the heater due to an oscillating ac power in it as a function of frequency, one can measure a certain combination of the specific heat and the thermal conductivity depending on the geometry of the heater. The frequency range covered was from 0.01 Hz to 5 kHz and it means that we had a frequency window of more than 5 decades. By using line and planar heaters, we were able to obtain the specific heat capacity, C_p, and the thermal conductivity, κ, of CKN independently. κ of CKN did not show any appreciable change or any frequency dependence in the whole glass transition region and $\kappa \approx 5.9$ mW/cmK.(ref. 8) This suggests that the heat carrying modes, probably high frequency phonons, are not affected at all by the glass transition.

In Fig. 1 shown are the real (C_p') and imaginary parts (C_p'') of the dynamic specific heat capacity of CKN versus log f (temperature oscillation frequency $f = \omega/2\pi$). As is easily seen from the data, the dynamics of the system slows down with decreasing temperature and the shape of C_p'' is asymmetrical. These features are typical of many glass formers; since it has been found that the

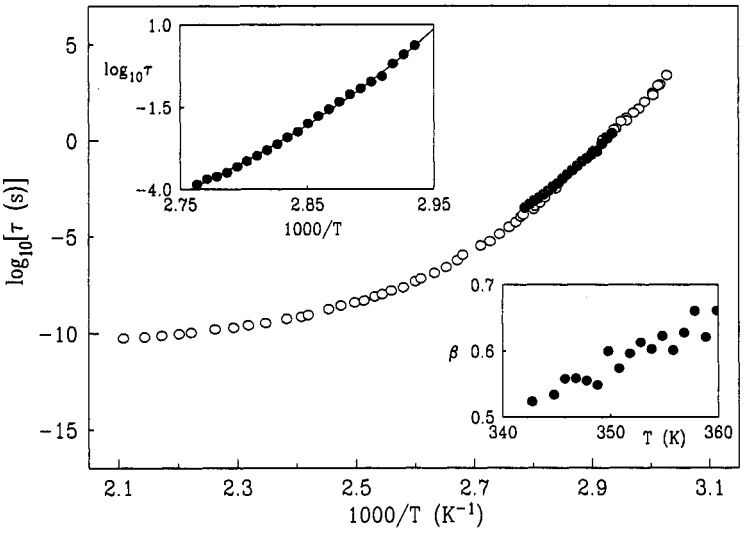

Fig. 2 The relaxation times of CKN, on a log scale, vs. T^{-1}. The solid circles denote the relaxation time from the dynamic specific heat capacity data, while the open circles do the shear relaxation times from Ref. 11. The upper inset displays the Vogel-Fulcher fit of τ from the dynamic specific heat data and the lower inset shows β as a function of T.

KWW (Kohlrausch-Williams-Watts) function $\phi(t) = \exp[-(t/\tau)^{\beta}]$ adequately describes the dynamics for them, the data at each temperature were fitted to Eq. (6) with

$$R(t) = \Delta C_p \exp[-(t/\tau)^{\beta}] \tag{8}$$

where $\Delta C_p = R(0)$ represents the relaxation strength. To enhance the precision we have used the set of real and imaginary data simultaneously in fitting; it is noted that since C_p^0 does not vary with T, the fitting was done with three parameters, i.e., ΔC_p, τ, and β. The best-fit curves drawn through the data indicate that the KWW function is reasonable in describing the enthalpy relaxation of CKN.

In the upper inset of Fig. 2, the relaxation time, τ, obtained from the fitting is shown against $1/T$. The data illustrate that τ is not behaving in an Arrhenius fashion, but in a Vogel-Fulcher one. The solid line represents the best fit to the data using the Vogel-Fulcher form, $\tau = \tau_0 \exp[\Delta/(T - T_0)]$. The fitting procedure yielded the values for parameters: $\tau_0 = 10^{-14.6}$ sec, $\Delta = 1800$ K, $T_0 = 288 \pm 8$ K. These are reasonable physical values and T_0 is probably close to the Kauzmann temperature. Although the crossover from a Vogel-Fulcher to an Arrhenius behavior at low temperatures was noted from the viscosity data,(ref. 9) we were not able to see the crossover in τ from our data. The lower inset of Fig. 2 shows the KWW fitting parameter β versus T. From the figure it is found that β varies linearly in T. The significance of this behavior is that the width of $C_p''(\omega)$ increases as T decreases and thus any analysis based upon the fact that $\beta = constant$, for instance time-temperature superposition, is not correct. This will also be of importance in analyzing the non-equilibrium data. It is of value to note that if we attempt the linear fitting of β versus T, we obtain, within experimental error, $\beta = \alpha(T - T_0)$ where α is a constant. With the reservation that the temperature range for the data is very far from T_0, it is worth pointing out that there exists a theory predicting such a behavior.(ref. 10) The relaxation strength, ΔC_p, also varies with T. Since C_p^0 remains constant for this particular system, the ΔC_p variation reflects the change in C_p^{∞} of the liquid, the significance of which is discussed below.

From our equilibrium measurements in CKN, we can test a very interesting idea of serial decoupling of various relaxing modes in the glass transition region.(ref. 11) The idea is that while on short time scales (or at high temperatures) the shear, volume, and enthalpy relaxation times are all the same, the shear modes decouple from the rest and the shear relaxation occurs at a faster rate as T is reduced toward the glass transition. To check the occurrence of decoupling, we plotted together, in Fig. 2, the enthalpy relaxation time (solid circles) and the shear relaxation time (= shear viscosity/ infinity-frequency shear modulus, open circles) taken from ref. 9. As is clear from the figure, the two kinds of relaxation times coincide reasonably well and no evidence of decoupling is seen within our time window. Thus if decoupling did indeed occur, it should do so at longer times than ~ 10 sec.

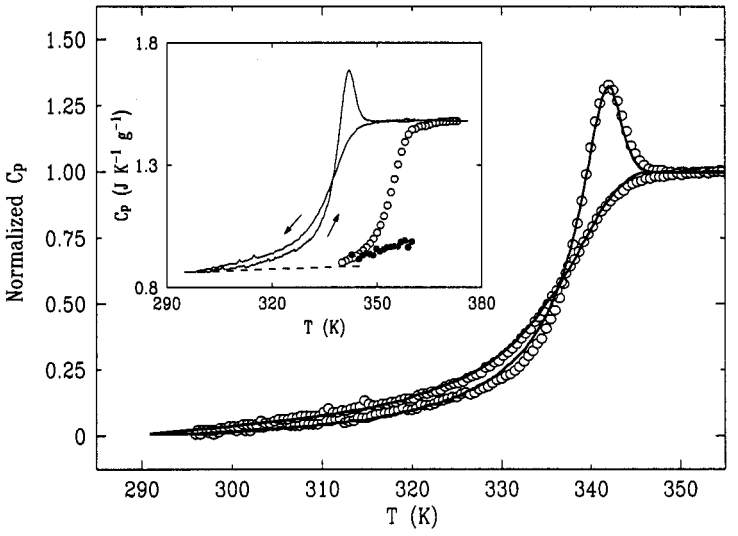

Fig. 3 The open circles denote the normalized specific heat capacity $[C_p(T) - C_{pg}(T)]/[C_{pl}(T_f) - C_{pg}(T_f)]$ and the solid lines are from the calculation. Inset shows the DSC data on cooling and heating at 10 K/min (solid lines) and the dynamic specific heat data at 100 Hz (circles). The dots in the inset denote C_p^∞ values of the equilibrium liquid, while the broken line does C_{pg}.

RATE-SCANNING EXPERIMENT RESULTS

As was mentioned above, one classical method to extract dynamic calorimetric information from a system is to perform rate-scanning experiments. Since the temperature variation in a scanning experiment may be regarded as a succession of small temperature jumps, one should be able to use Eq. (3) in describing the results. In the inset of Fig. 3, we show the DSC trace (solid lines) of CKN, as a function of T, taken at cooling and heating rates of 10 K/min with a Perkin-Elmer DSC-7 calorimeter. The DSC data on cooling show a typical transition from the value of the liquid specific heat capacity (C_{pl}) at high temperatures to that of the glass specific heat capacity (C_{pg}) at low temperatures while the data on heating are the result of the system recovering equilibrium. For comparison we have overlayed the dynamic specific heat capacity measured at 100 Hz (open circles). Also plotted as solid circles in the figure is C_p^∞ from the KWW fitting of $C_p(\omega)$. It should be noticed that C_p^∞ varies with T while C_{pg} does not show any appreciable variation as illustrated by the broken line in the figure. This can be understood if we remember that C_p^∞ is the specific heat capacity of the *equilibrium* liquid probed at high frequency and thus the structure of the liquid, which appears frozen to high frequency thermal excitation, continues to change with T while that of the glass does not vary much in T.

To understand the DSC results, we recall that the essence of the data lies in the broken stationariness; as the system is cooled at constant rate, the characteristic time of the relaxing modes gets longer and at some point the relaxing modes split off from other fast degrees of freedom which set the system temperature, T. (The converse is true in the case of heating.) To deal with this situation in a phenomenologically simple way, the configurational (or fictive) temperature T_f, which itself is a function of T, is defined through

$$H(T) = H_l(T_f) - \int_T^{T_f} C_{pg}(T')\,dT' \tag{9}$$

where $H(T)$ is the measured enthalpy and $H_l(T)$ is the enthalpy of the equilibrium liquid.(ref. 12,13) Since C_{pg} represents the contribution mostly from the fast degrees of freedom, Eq. (9) states that the enthalpy due to the relaxing modes is that at T_f while the temperature of the fast degrees of freedom is T. Thus, T_f signifies the temperature of the structural configuration of the relaxing modes. It is easy to show that dT_f/dT is the normalized heat capacity due to the relaxing components,

$$dT_f/dT = [C_p(T) - C_{pg}(T)]/[C_{pl}(T_f) - C_{pg}(T_f)]\,. \tag{10}$$

Then, noting that the relaxation strength ΔC_p in the nonequilibrium situation is determined by the configuration temperature, C_{pg} is due to the fast degrees of freedom, and $R(t) = \Delta C_p\,\phi(t)$, Eq. (3) is transformed to the one for T_f (ref. 14)

$$T_f(t) = T_i + \int_0^t [1 - \phi(t,t')]\delta\dot{T}(t')\,dt' \tag{11}$$

where T_i is a temperature at which a given experiment begins.

To evaluate Eq. (11), one need to specify $\phi(t,t')$ which, however, is known only for equilibrium situations, where $\phi(t,t') = \phi(t-t') = \exp[-((t-t')/\tau)^\beta]$. Moynihan *et al.* (ref. 12) developed a theory, building on previous works,(ref. 15) to deal with this situation and had great successes in interpreting their DSC data of various glass-forming materials. However, one of the key assumptions they made in the absence of the equilibrium data, that is, β is constant, does not seem to be valid and therefore the theory must be improved. Since we do not have a universally accepted theory for the equilibrium KWW function not to mention the nonstationary case, we resort to the idea of distribution of relaxation times and seek to extend it. The KWW function is expressed as

$$\exp[-(\frac{t-t'}{\tau})^\beta] = \int d\tau_D g(\tau_D) \exp(-\frac{t-t'}{\tau_D}) \tag{12}$$

where $g(\tau_D)$ is the distribution function. Now we assume that the characteristics of the relaxation function, β and τ, are determined by T_f, since T_f is the effective temperature of the relaxing modes. That is,

$$\beta = \alpha(T_f - T_0) \quad ; \quad \tau = \tau_0 \exp[\frac{1}{T}(\frac{\Delta}{1-T_0/T_f})] \tag{13}$$

if T_f deviates from T. The latter assumption of Eq. (13) can be justified, as first shown by Scherer,(ref. 16) by remembering the Adam-Gibbs theory:(ref. 17) $\tau = \tau_0 \exp[const/TS_c]$ where S_c is the configurational entropy of the system. Thus the temperature dependent barrier $\Delta/(1-T_0/T)$ of the Vogel-Fulcher law is determined by S_c and if $T \neq T_f$, T_f determines $S_c(T_f)$ which in turn fixes the barrier.

The distribution of the relaxation times can be represented either by the prefactor distribution with the barrier given by $S_c(T_f)$ or by the barrier distribution around $\Delta/(1-T_0/T_f)$. While the physical interpretation of the former representation is not easy compared to the latter, it gives the best results and so we used the former in the present calculation. Now that each τ_D is time-dependent via T_f, each Debye relaxation of Eq. (12), $\exp[-(t-t')/\tau_D]$, is replaced by $\exp[-\int_{t'}^{t} dt''/\tau_D(t'')]$. Note that this is equivalent to assuming the exponential decay at each instant with τ_D of that moment. The time-varying nature of β due to its temperature dependence is taken into account by making the distribution function $g(\tau_D)$ time-dependent. (It is reminded again that nonlinearity is caused by the time dependence of τ and β of the relaxation function.) With these ingredients, we solve numerically Eq. (11) with the same constraint (scanning rate) as in actual experiments and calculate dT_f/dT. The results are shown, as thick solid lines, in Fig. 3 along with the properly normalized data points. The coincidence is striking. The main features of the rate-scanning, cooling as well as heating, data are faithfully reproduced. We have also calculated for the cases with different thermal histories with equal success.

TIME DOMAIN TEMPERATURE RELAXATION

In time domain dynamic calorimetry, a certain amount of heat is applied instantaneously to a sample and its temperature response is examined in real time. Initially applied heat is distributed only among phonon degrees of freedom causing an instantaneous temperature jump, and then part of energy slowly diffuses into the configurational degrees of freedom resulting in the decrease of the sample temperature. Thus, this temperature relaxation experiment is the time domain counterpart of the modulation calorimetry. While it is not easy to apply a large amount of power to a sample in modulation calorimetry, there is no difficulty in varying the temperature jump sizes in time domain dynamic calorimetry. This feature of the time domain method allows one to study nonlinear temperature relaxation. To properly carry out the time domain experiment, maintenance of the adiabatic condition during the whole period of temperature relaxation is essential. Since the space is limited, we shall only present the schematic diagram of the adiabatic calorimeter used in the present investigation in Fig. 4. The detailed description is given in our recent publications.(ref. 18)

We briefly outline, as an example, how the experiment of 1 K temperature jump is conducted. Initially at $t = 0$ the pre-calculated amount of power, corresponding to 1 K increase in temperature,

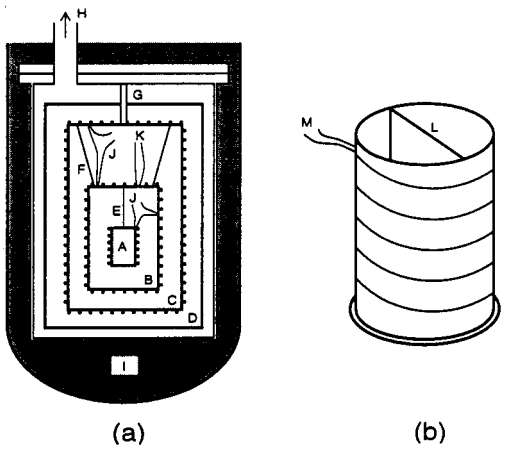

Fig. 4 Schematic diagrams of (a) the adiabatic calorimeter and (b) the sample cell: (A) the sample cell filled with CKN, (B) inner adiabatic shield, (C) outer adiabatic shield, (D) radiation shield, (E) manganin suspending wire, (F) stainless steel suspending wire, (G) stainless steel supporting tube, (H) vacuum line, (I) liquid nitrogen, (J) copper-constantan differential thermocouple, (K) E-type thermocouple, (L) partition, (M) manganin heater wire. The heating wires are wound around A, B, and C to control temperatures. Heat is injected to the sample assembly A, and the temperature of the shield B is controlled to maintain adiabatic conditions.

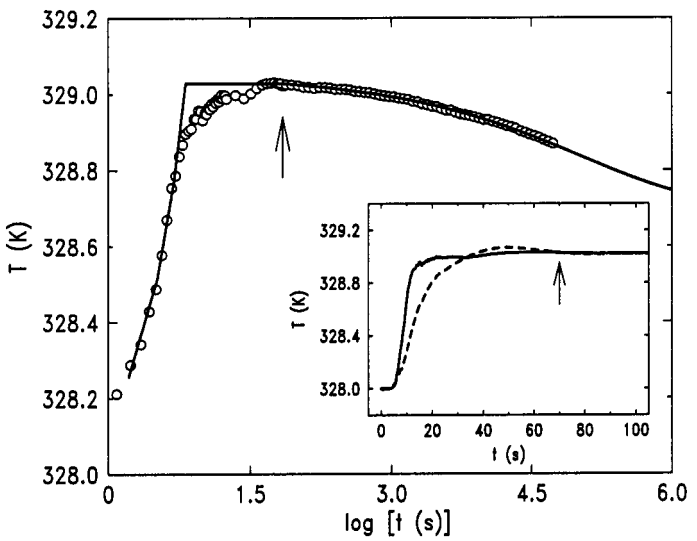

Fig. 5 Time domain relaxation experiment with CKN: Inset illustrates the temperature variations of the sample (solid line) and the inner shield (broken line) at early times following the injection of heat into the sample and shield. When the temperature of the shield overshoots, the temperature controlling action for the inner shield begins. The adiabatic condition is achieved (arrows) after the transient period elapses. The circles in the figure represent the data and the line is drawn from the calculated values; they show excellent agreement. Notice the logarithmic scale in the time axis.

is applied to the inner shield for 10 seconds and then power is turned off. At $t = 5$ s, the amount of power needed to raise the sample temperature by 1 K is supplied for 5 seconds. The temperature variations of the sample (solid line) and the inner shield (broken line) caused by these power inputs are shown in the inset of Fig. 5. Between $t = 10$ s and the time at which the temperature of the shield overshoots, the power input to the inner shield stays zero. But after this moment the temperature controlling action for the inner shield begins. The adiabatic status is achieved after the transient period of approximately 1 minute elapses, as indicated in the figure by the arrows. In order to ascertain that the time domain experiment can be understood within the same theoretical framework as the one used in the scanning experiment, we again calculate the temperature evolution according to Eq. (11). However, this time we are in an adiabatic situation and Eq. (10) becomes

$$-C_{pg}(T)dT = [C_{pl}(T_f) - C_{pg}(T_f)]dT_f . \tag{14}$$

The solid line in Fig. 5 represents the result of calculation with Eq. (11) and (14). Of course, in the early times before the adiabatic condition is set in, the nonadiabatic effect was taken into account in the calculation. The agreement between the data and the calculated values is excellent and this demonstrates the nonstationary nature of the temperature relaxation.

Finally, in order to examine the possible nonlinear effects from the higher order terms in the response equation, we have conducted the time domain experiments with initial temperature

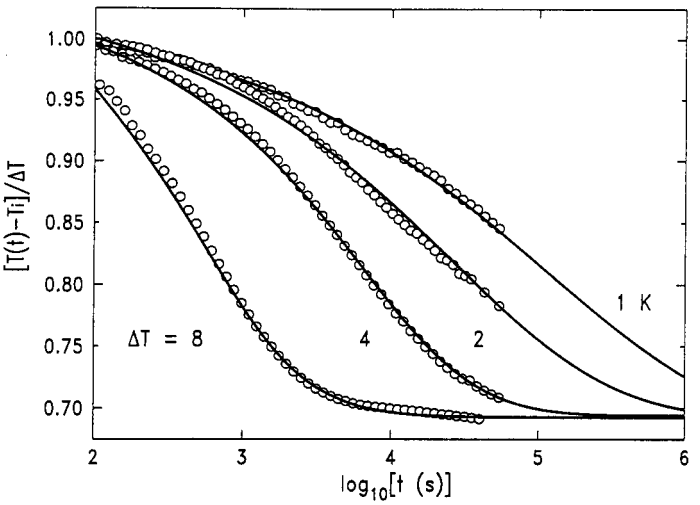

Fig. 6 Nonlinear temperature relaxation of CKN. Initially the system is at T_i = 328 K, and sudden temperature jumps of magnitude ΔT = 1, 2, 4, and 8 K are induced by applying pre-calculated amounts of power to the cell and the inner shield. After the transient period elapses, the adiabatic relaxation of temperature follows. The nonlinear nature of the relaxation is fully accounted for, as indicated by solid lines, by using the nonstationary response function.

jumps of various magnitude. ΔT = 1, 2, 4, and 8 K were induced at T_i = 328 K and the ensuing temperature variations were monitored. The strong nonlinear nature of the temperature relaxation of supercooled CKN is evident as illustrated in Fig. 6. However, this nonlinear nature of the relaxation can be accounted for by allowing β and τ of the KWW function, equilibrium response function, to vary in the course of relaxation. The lines in Fig. 6 were calculated using Eq. (11) and (14) as previously explained and the excellent agreement persists even for the largest step experiment. Thus, we conclude all the nonlinear effect in the enthalpy relaxation in supercooled CKN is due to the broken stationariness.

CONCLUSIONS

In conclusion, we have extensively investigated equilibrium and nonequilibrium, linear and nonlinear enthalpy relaxation of supercooled CKN. It was shown that the glass transition is basically a phenomenon due to the splitting-off of the slow relaxing modes from the rest and the associated nonstationary relaxation can be described in the theoretical framework for the equilibrium relaxation if the latter is properly modified. The nonstationary description holds even for the relaxation following a 8 K temperature jump. This work was supported by RCDAMP of Pusan National University and the BSRI of Pohang University of Science and Technology.

REFERENCES

1. See, for example, J. Wong and C. A. Angell, *Glass structure by spectroscopy* (Marcel Dekker, New York, 1976).
2. E. Leutheusser, *Phys. Rev. A* **29**, 2765 (1984).
3. W. Kauzmann, *Chem. Rev.* **43**, 219 (1948).
4. O. Nakada *J. Phys. Soc. Japan* **15**, 2280 (1960).
5. R. Kubo, *Rep. Prog. Phys.* **29**, 255 (1966).
6. D. H. Jung et al., *Meas. Sci. Technol.* **3**, 475 (1992); I. K. Moon, Y. H. Jeong, and S. I. Kwun, *Rev. Sci. Instrum.* **67**, 29 (1996).
7. N. O. Birge and S. R. Nagel, *Rev. Sci. Instrum.* **58**, 1464 (1987).
8. Y. H. Jeong and I. K. Moon, to be published.
9. H. Tweer et al., *J. Am. Ceram. Soc.* **54**, 121 (1971).
10. M. Papoular, *Philos. Mag. Lett.* **64**, 421 (1991).
11. C. A. Angell, *J. Noncryst. Solids* **131-133**, 13 (1991).
12. C. T. Moynihan et al., *Ann. N. Y. Acad. Sci.* **279**, 15 (1976).
13. J. Jäckle, *Physica* **127B**, 79 (1984).
14. G. W. Scherer, *Relaxations in glass and composites* (Wiley, New York, 1986).
15. O. Narayanaswamy, *J. Am. Ceram. Soc.* **54**, 491 (1971).
16. G. W. Scherer, *J. Am. Ceram. Soc.* **67**, 504 (1984); I. M. Hodge, *Macromolecules* **19**, 936 (1986).
17. G. Adam and J. H. Gibbs, *J. Chem. Phys.* **43**, 139 (1965).
18. I. K. Moon and Y. H. Jeong, *Rev. Sci. Instrum.* **67**, 3553 (1996); Y. H. Jeong, *Thermochim. Acta* in press (1997).